Projecting Stratocumulus Transitions on the Albedo—Cloud Fraction Relationship Reveals Linearity of Albedo to Droplet Concentrations

Tom Goren[1] ⓘ, **Graham Feingold**[2] ⓘ, **Edward Gryspeerdt**[3] ⓘ, **Jan Kazil**[2,4] ⓘ, **Jan Kretzschmar**[1] ⓘ, **Hailing Jia**[1] ⓘ, and **Johannes Quaas**[1] ⓘ

[1]Institute for Meteorology, Leipzig Universität, Leipzig, Germany, [2]Chemical Sciences Laboratory, NOAA, Boulder, CO, USA, [3]Space and Atmospheric Physics Group, Imperial College London, London, UK, [4]Cooperative Institute for Research in Environmental Sciences, University of Colorado, Boulder, CO, USA

Abstract Satellite images show solid marine stratocumulus cloud decks (Sc) that break up over the remote oceans. The Sc breakup is initiated by precipitation and is accompanied by a strong reduction in the cloud radiative effect. Aerosol has been shown to delay the Sc breakup by postponing the onset of precipitation, however its climatic effect is uncertain. Here we introduce a new approach that allows us to re-cast currently observed cloud cover and albedo to their counterfactual cleaner world, enabling the first estimate of the radiative effect due to delayed cloud breakup. Using simple radiative approximation, the radiative forcing with respect to pre-industrial times due to delayed Sc breakup is -0.39 W m^{-2}. The radiative effect changes nearly linearly with aerosol due to the droplet concentration control on the cloud cover, suggesting a potentially accelerated warming if the current trend of reduction in aerosol emissions continues.

Plain Language Summary The response of cloud cover to aerosol is a climatologically important quantity that has been extremely difficult to estimate. The challenge is that one would need to estimate the fractional area that is currently overcast, but which would have been partly overcast in a cleaner atmosphere. Global climate models (GCMs) are one tool to address such a problem. They allow one to change aerosol levels and to evaluate the cloud response. However, representation of warm, low-level cloud processes, and in particular aerosol-cloud interactions in GCMs, is inadequate. Here we introduce an observational method that allows us to re-cast the currently observed cloud cover and albedo of oceanic warm clouds to their counterfactual state in a cleaner world. We find a linear relationship between the cloud radiative effect and droplet concentration. If we continue to experience a decrease in aerosol emissions then we anticipate a reduction in the aerosol-cloud radiative effect. The global annual radiative forcing associated with anthropogenic aerosol delaying closed cell breakup is found to be -0.39 W m^{-2}.

1. Introduction

The spatial coverage of clouds and their degree of reflectivity exert significant control over the energy budget of the Earth (Slingo, 1990). Despite numerous studies that have investigated the aerosol effect on cloud radiative properties, large uncertainty remains with respect to how the global low cloud radiative effect has changed since pre-industrial, pristine levels (Carslaw et al., 2013; Forster et al., 2021; Kretzschmar et al., 2017; Stevens, 2015). Typically, an increase in aerosol number concentration (N_a) increases the cloud droplet number concentration (N_d). As a result, the cloud radiative properties change due to changes in the cloud albedo, liquid water path (LWP) and coverage (Albrecht, 1989; Twomey, 1977). The cloud albedo response to changes in N_d, assuming constant cloud water amount (Twomey, 1977), has drawn much attention in recent decades. It proposes a non-linear dependence of the cloud albedo on N_d, so that the sensitivity of cloud albedo to N_d weakens with increasing N_d (Twomey, 1991). Since the scene mean albedo, $\overline{\alpha}$ (i.e., including the fractional coverage of clouds in a given scene, f_c), is a nearly linear function of f_c (Bender et al., 2011; Schneider & Dickinson, 1976), a relationship between N_d and f_c (Bretherton et al., 2010; Goren & Rosenfeld, 2014; Goren et al., 2019; Rosenfeld et al., 2006, 2019; Sharon et al., 2006; Wang & Feingold, 2009; Wood et al., 2011) means a nearly linear response of $\overline{\alpha}$ to N_d.

The climatology of marine warm clouds exhibits a geographical dependence, with high f_c in the eastern subtropical oceans in proximity to the major continents that decreases westward (Wood, 2012). The geographical

distribution of f_c is a manifestation of the stratus-to-cumulus (Bretherton & Wyant, 1997; Wyant et al., 1997) and closed-to-open cell transitions (Rosenfeld et al., 2006) of marine stratocumulus clouds (Sc). The closed-to-open cell transitions have been shown by numerous studies to be initiated by the formation of precipitation (Rosenfeld et al., 2006; Wang et al., 2010; Wang & Feingold, 2009). The precipitation causes rain-driven downdrafts that collide with one another as they diverge at the ocean surface. This leads to the formation of cumulus clouds in the convergence zones that eventually replace the closed cells (Feingold et al., 2010). The transition to open cells lowers f_c and exerts a significantly smaller cloud radiative effect (CRE), defined as the difference in shortwave radiation with respect to cloud-free conditions (Goren & Rosenfeld, 2014). The other common type of Sc transition that shapes the climatology of marine warm clouds is the stratus-to-cumulus transition. The latter is driven by the advection of the Sc toward increasingly warmer sea surface temperature (SST) and the simultaneous deepening and decoupling of the marine boundary layer (MBL). The increasing SST promotes formation of cumulus clouds that rise through the decoupled stratus layer above, thereby increasing the turbulent kinetic energy and mixing at cloud top that eventually dissipate the status layer (Bretherton & Wyant, 1997; Wyant et al., 1997).

Studies have shown that aerosol can delay precipitation, thereby delaying the time of the transition from closed-to-open cells (Goren et al., 2019). The role of aerosol in modulating the timing of the stratus-to-cumulus transition is still ambiguous (Bretherton & Wyant, 1997; Yamaguchi et al., 2017), although recent studies provide stronger evidence that precipitation does play a significant role in determining the timing of the transitions (Christensen et al., 2020; Diamond et al., 2022; Yamaguchi et al., 2017). If aerosol does affect the timing of the Sc breakup, the geographical location of the Sc breakup is expected to be shifted westward in events that are more polluted (Goren et al., 2019). This is due to the persistent winds (Wood, 2012) that continuously advect the Sc and aerosol.

Here, we present a cloud physical metric that accounts for the deficit or surplus of the observed cloud water amount from that needed to form precipitation, ΔLWP. A relationship between ΔLWP, $\overline{\alpha}$ and f_c emerges for Sc, and allows us to re-cast satellite observations of $\overline{\alpha}$ and f_c to their equivalent in a lower N_d world. This provides us the ability to explore the fundamental response of the Sc f_c, and the subsequent cloud radiative effect, to changes in aerosol emissions, represented here by N_d.

2. Methods

2.1. Deficit and Surplus of Cloud Water as a Measure of Temporal and Spatial Cloud Evolution

In an adiabatic cloud parcel the adiabatic liquid water content (LWC) increases nearly linearly with height (H) above cloud base:

$$\text{LWC} = C_w H \tag{1}$$

with the adiabatic condensation coefficient C_w (Brenguier et al., 2000) of a typical value of $C_w = 1 \, \text{m g m}^{-4}$. Vertical integration, assuming height-independent C_w, yields:

$$\text{LWP} = \frac{1}{2} C_w H^2. \tag{2}$$

Combining (Equation 1) and (Equation 2) gives:

$$\text{H}^2 \propto LWC^2 \propto LWP_{adi}. \tag{3}$$

Assuming that the bulk of droplet activation occurs just above cloud base so that N_d remains roughly constant with height, the LWC dependence on effective radius, r_e, and N_d is as follows:

$$\text{LWC} \propto r_e^3 N_d. \tag{4}$$

By combining (Equation 3) and (Equation 4) we obtain

$$\text{LWP}_{adi} \propto r_e^6 N_d^2, \tag{5}$$

and assuming a critical r_e of 15 μm for initiation of drizzle (Chen et al., 2008; Freud & Rosenfeld, 2012; Gerber, 1996; Goren et al., 2019; Rosenfeld et al., 2012; VanZanten et al., 2005), r_{e_c}, an equivalent critical LWP, LWP_c can be defined:

$$LWP_c \propto r_{e_c}^6 N_d^2. \tag{6}$$

Equation 6 shows that the higher N_d, the deeper the clouds need to be in order to initiate drizzle. We define ΔLWP, the LWP deficit or surplus, in the following way:

$$\Delta LWP = LWP_c - LWP_{obs}, \tag{7}$$

which serves as a metric that characterizes the microphysical distance of the clouds, in terms of LWP, from the point of initiation of precipitation. Following this.

ΔLWP > 0 g m^{-2} characterizes non precipitating clouds, ΔLWP < 0 g m^{-2} characterizes precipitating clouds, and ΔLWP = 0 g m^{-2} is the precipitation initiation point. LWP_c is calculated in the following way (see method section for more details):

$$LWP_c = 0.033 \times N_d^2. \tag{8}$$

2.2. Examining the ΔLWP Metric in Large Eddy Simulations

Figure 1a demonstrates the concept of ΔLWP for large eddy simulations (LES) of a closed-to-open cell transition under varying initial N_a. The simulations were performed for an observed closed-cell event that formed within a European polluted air mass that gradually cleansed until the clouds broke up into open cells (for more details refer to Goren et al. (2019)). The simulations represent a typical Sc trajectory of closed cells advecting from the coastal region toward the remote pristine ocean. The figure shows the simulated LWP that corresponds to the "observed" (actual modeled) LWP along the cloud trajectory, as well as curves of LWP_c calculated for simulations with different initial N_a (all else equal). A key feature in the Figure is that curves of LWP_c systematically intercept the real LWP (blue line) sooner for cleaner simulations (i.e., lower initial N_a). It can be seen that ΔLWP (illustrated by the vertical arrows for NA225) decreases with time during the course of the cloud evolution. This leads to the notion that ΔLWP can be thought of as a vector that points to the microphysical status of the clouds with respect to the precipitation initiation point.

2.3. Time—Space Equivalence

Sandu et al. (2010) have shown that spatial gradients in mean field properties in Sc regions resemble the temporal changes of Sc Lagrangian trajectories. This is due to the persistent sub-tropical highs (Sandu et al., 2010; Wood, 2012) and cloud controlling factor gradients, such as boundary layer height, sea surface temperature (Bretherton & Wyant, 1997) and subsidence rate (Sandu et al., 2010), which are determined to a great extent by the distance from the coasts. Given that the wind flow is rather persistent due to the sub-tropical highs, the continuous formation of Sc that are advected by the sub-tropical winds along their trajectory toward the remote pristine ocean, where they often breakup (Wood, 2012), allows the time and space equivalence assumption. This is manifested by the Sc climatology, which shows a consistent decrease of cloud cover from the coastal regions toward the remote pristine oceans, along with a decrease in r_e and an increase in N_d, accompanied by an increasing frequency of drizzling clouds (see review of Sc by Wood (2012)). The Lagrangian LES presented in the previous section supports the time-space equivalence assumption, in which case as the time axis in Figure 1a would be the distance from the coast (see arrow in Figure 1b representing the simulated clouds trajectory).

2.4. Examining the ΔLWP Metric in Satellite Data

We define persistent Sc clouds as regions where warm, low level oceanic clouds exist at least 40% of the time annually (see Figure S1 in Supporting Information S1 for frequency of occurrence map). The cutoff of 40% was chosen as being the global median occurrence of warm low level clouds, as calculated from our data (see Section 1 in the Supporting Information S1 for data description (Bennartz & Rausch, 2017; D. Grosvenor & Wood, 2014;
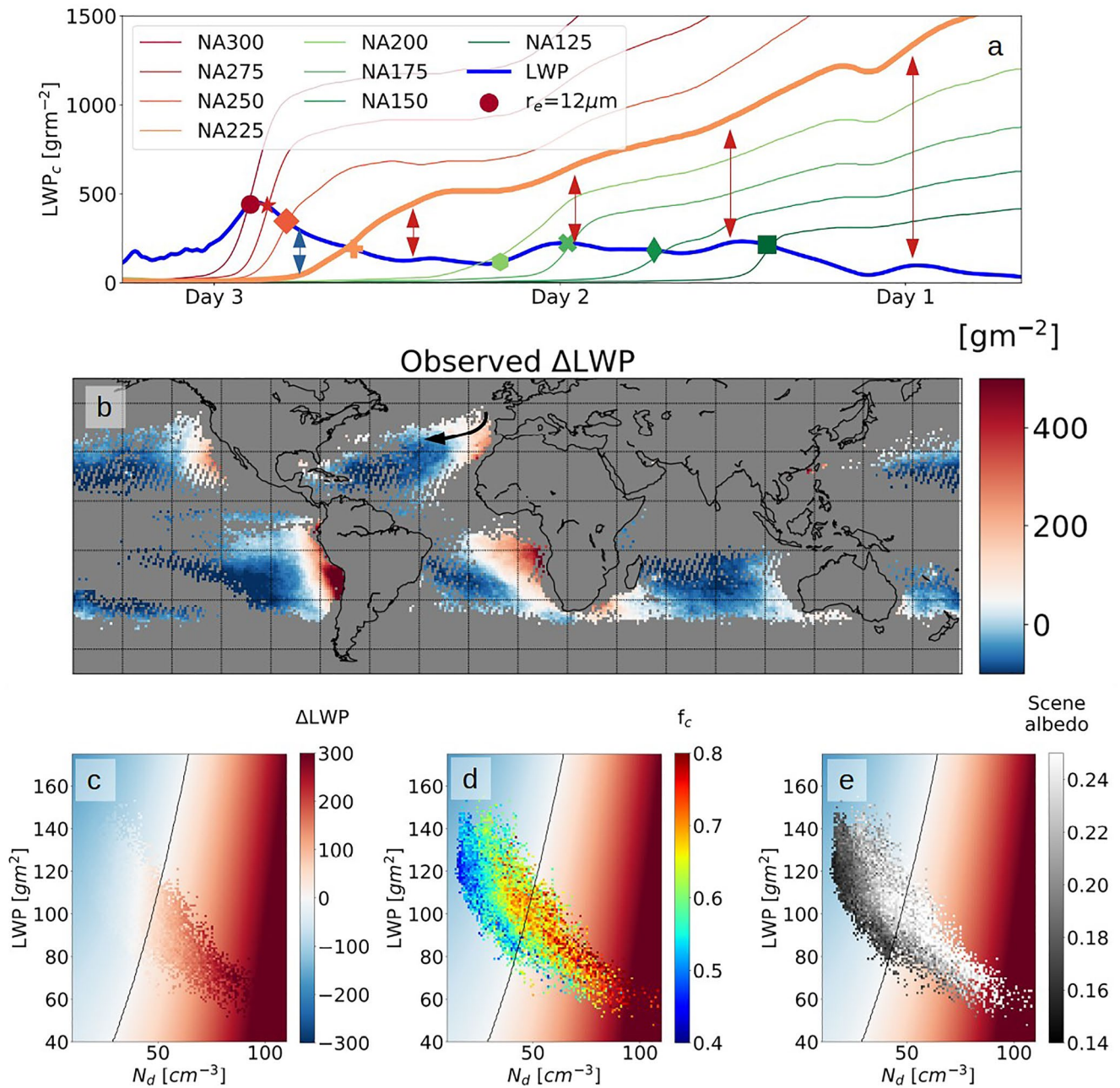
Figure 1. Linking Δliquid water path (LWP) to stratocumulus cloud decks (Sc) temporal evolution. (a) Time series taken from the Lagrangian large eddy simulations of closed-to-open cells transition, with varying initial N_a, for a case study that was observed over the eastern north Atlantic ocean (Goren et al., 2019). In blue is the actual modeled LWP (i.e., similar to the observed LWP). Also shown are LWP_c curves (calculated using the simulated N_d and Equation 8) for simulations with lower initial N_a, assuming all else equal. Symbols indicate the time when $LWP_c = LWP$ and $r_e = 12$ μm (an r_e in the range of 12–16 μm is an indication of significant drizzle (Gerber, 1996; Rosenfeld et al., 2012), and when the simulated clouds start to break up. Each symbol and color represents different simulations with different initial N_a, for example, red points represent NA300 with initial N_a of 300 cm^{-3}. Note the monotonic delay in cloud breakup associated with increasing initial N_a. ΔLWP is illustrated by the vertical arrows for NA225 (orange curve), which become smaller with time. (b) A map of ΔLWP climatology for Sc in regions where clouds are observed at least 40% of the time annually and from which the data for the analysis is derived. Black arrow shows the Lagrangian trajectory shown in (a). (c, d, and e) show the observed ΔLWP, f_c and $\bar{\alpha}$, respectively, overlaying the theoretical ΔLWP calculated for every combination of N_d and LWP (contours). Note that the background of d and e follows the colorbar of (c).

D. P. Grosvenor et al., 2018; Khairoutdinov & Randall, 2003; Platnick et al., 2003; Sourdeval et al., 2016; Quaas et al., 2006; Wielicki et al., 1996)). A 40% cutoff is also in accordance with the occurrence of Sc in the major Sc regions (Muhlbauer et al., 2014; Wood, 2012). Figure 1b shows the ΔLWP climatology of Sc (solid and broken Sc) comprising 10 years of Moderate Resolution Imaging Spectroradiometer (MODIS) data, where posi-
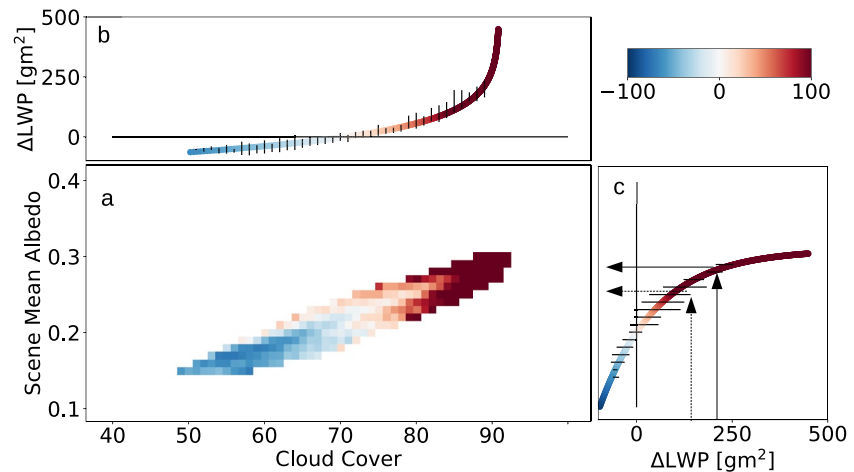
Figure 2. Relationship between $\overline{\alpha}$, f_c and Δliquid water path (LWP). (a) A joint histogram showing the relationship between stratocumulus cloud decks climatology of $\overline{\alpha}$ versus f_c with the mean ΔLWP in color. A linear dependence of $\overline{\alpha}$ on f_c can be seen, while ΔLWP depends on both. (b and c) show the exponential fitting between ΔLWP to f_c and $\overline{\alpha}$, respectively, referred to as ΔLWP kernels. Black lines shows ±1 standard deviation of ΔLWP. The difference in $\overline{\alpha}$ with respect to a counterfactual cleaner world is illustrated by the arrows in (c): the solid (dashed) arrow illustrates the observed (counterfactual cleaner world) ΔLWP and the respective observed (recast) $\overline{\alpha}$.

tive (negative) ΔLWP are associated with overcast (broken) Sc (see also Figure 1d). The climatology of ΔLWP establishing the applicability of the theoretical ΔLWP (Section 2.1) is further shown in Figures 1c–1e. The Figure shows the Sc climatology of ΔLWP, f_c, and $\overline{\alpha}$ on the LWP-N_d plane. The black line indicates $r_e = 15$ μm, where ΔLWP $= 0$ g m^{-2}, and separates between overcast and broken clouds (Figure 1d), and between high and low $\overline{\alpha}$ (Figure 1e). It expresses the bifurcation of Sc, that is, the tendency of Sc to exist in either solid or broken regimes (Baker & Charlson, 1990; Koren & Feingold, 2011).

Figure 2a shows the relationship between f_c and $\overline{\alpha}$ for the Sc climatology, with ΔLWP represented by the color scale. The near linear relationship between $\overline{\alpha}$ and f_c is expected in Sc clouds when temporally averaging the cloud properties (Bender et al., 2016; Engström et al., 2015), and means that the variability in $\overline{\alpha}$ is primarily controlled by f_c. The near-linear relationship is also expected from physical considerations, as Sc are capped by an inversion that deepens relatively little as the clouds widen (Feingold et al., 2017). It can be further seen that ΔLWP changes simultaneously with f_c and $\overline{\alpha}$, so that the climatological Sc breakup occurs around f_c of 75% (assuming that ΔLWP $= 0$ g m^{-2} indicates drizzle initiation and cloud breakup). Furthermore, the decreasing ΔLWP from being high and positive for high f_c, to being low and negative for low f_c, implies that the life cycle of Sc, from overcast to broken clouds, progresses along the $\overline{\alpha}$ - f_c curve. The dependence of ΔLWP on f_c and $\overline{\alpha}$ separately, is shown respectively in Figures 2b and 2c. The relationships (hereafter kernels) are used to relate a given ΔLWP to its associated f_c and $\overline{\alpha}$, as explained in the following section. The kernel parameters are provided in Section 5.1 in Supporting Information S1.

2.5. Recasting Cloud Cover and Albedo to a Counterfactual Cleaner World

For simplicity, we refer to the global Sc climatology as if it were an instantaneous global Sc scene. This simplification is supported by the persistent meteorology and synoptic flow in areas that favor Sc (Muhlbauer et al., 2014; Sandu et al., 2010; Wood, 2012). The respective changes in $\overline{\alpha}$ and f_c are therefore calculated for the climatology of Sc. This is done by leveraging the ΔLWP concept in a way that allows us to cast $\overline{\alpha}$ and f_c to a counterfactual lower N_d scenario. To do so we calculate the clean-world ΔLWP (ΔLWP$_{cln}$) by assuming a fractional change in N_d and calculating thereafter LWP$_{c-cln}$ using Equation 8 to get ΔLWP$_{cln}$. We assume no change in the observed LWP, that is, similar meteorology in the real and counterfactual worlds:

$$\Delta LWP_{cln} = LWP_{c-cln} - LWP_{obs}. \tag{9}$$

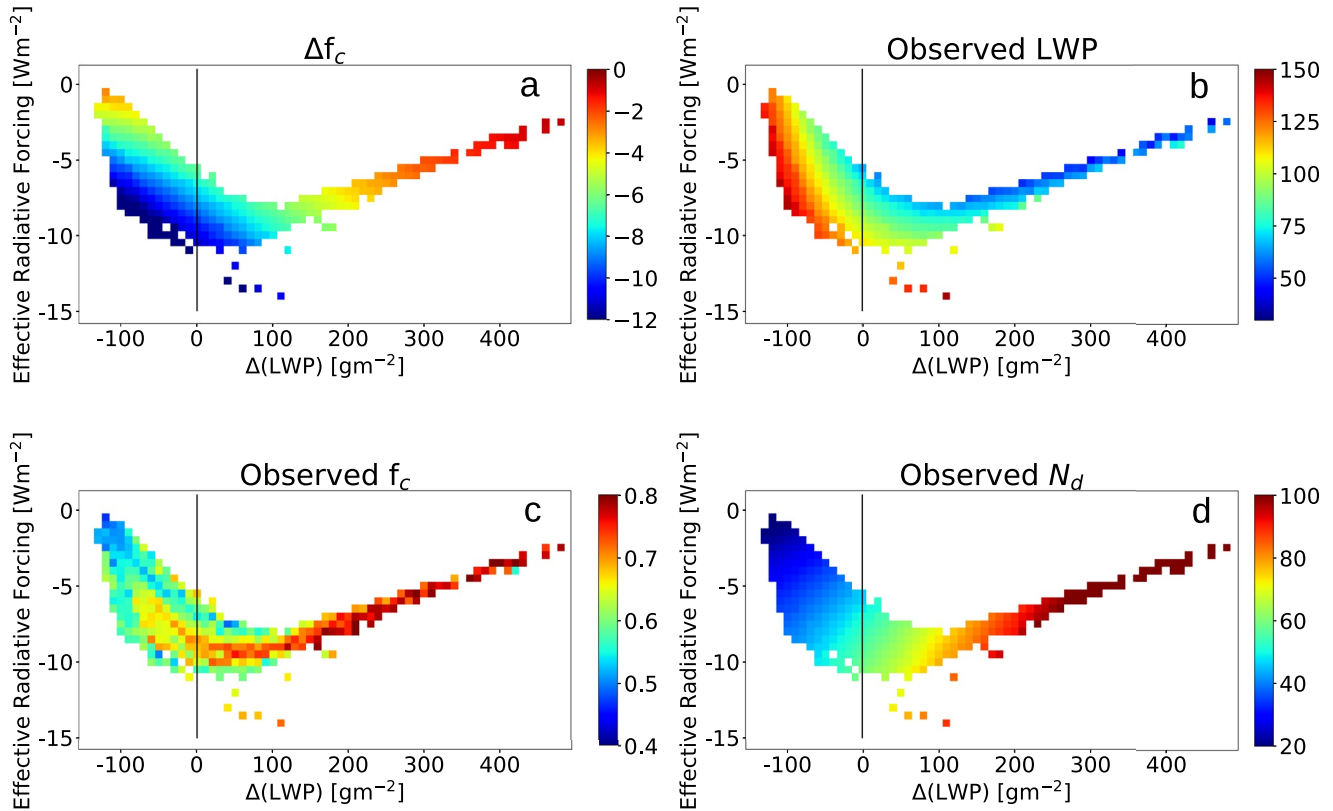## Effective Radiative Forcing vs Δ(LWP) Assuming 80% of the Observed N$_d$

Figure 3. Dependence of ERF$_{aci}$ on Δliquid water path (LWP). N$_{aci}$ is calculated for a world consisting 80% of the observed ERF$_d$. In color are (a) Δf$_c$, (b) observed LWP, (c) observed f$_c$ and (d) observed N$_d$. The ERF$_{aci}$ becomes smaller (i.e., less negative) toward high ΔLWP due to the weakening of the first indirect effect at higher N$_d$. Toward low ΔLWP, the ERF$_{aci}$ becomes smaller (i.e., less negative) due to lower observed N$_d$, which means smaller fractional change in N$_d$, as well as due to the lower f$_c$ that limits the effectiveness of the first indirect effect. Also note how Δf$_c$ becomes more negative for ΔLWP < 0 g m^{-2} (a) when cloud breakup occurs.

The difference in the radiative effect between the two scenarios is then calculated by converting the difference between the observed ΔLWP, ΔLWP$_{obs}$, and ΔLWP$_{cln}$, to a change in $\overline{\alpha}$ and f$_c$, Δ$\overline{\alpha}$ and Δf$_c$, respectively (see illustration for Δ$\overline{\alpha}$ in Figure 2c). The effective radiative forcing due to aerosol-cloud interactions, ERF$_{aci}$ (Boucher et al., 2013), represents here both the first indirect effect (Twomey, 1977) and the cloud cover adjustments (Albrecht, 1989). The LWP adjustments are not accounted for, as we assume no change in LWP between the observed and counterfactual world (Equation 9).

3. Results

3.1. Exploring the Cloud Radiative Effect Response to N$_d$ Using ΔLWP

We now show the fundamental response of $\overline{\alpha}$ and f$_c$ to changes in N$_d$ by assuming an hypothetical atmosphere containing 80% of the currently observed N$_d$ (e.g., for a given observed N$_d$ = 100 cm^{-3}, an N$_d$ fraction of 80% means N$_d$ = 80 cm^{-3}). Figure 3 synthesizes the response in terms of the ERF, defined here as the change in energy flux caused by anthropogenic aerosol emissions affecting the cloud radiative properties, versus ΔLWP. An asymmetric V-shape can be seen, with a minimum (i.e., maximum negative ERF) ranging between ΔLWP = 0–150 g m^{-2}. As ΔLWP decreases and approaches 0 gm^{-2}, LWP (Figure 3b) and MBL depth (not shown) increase, and Δf$_c$ becomes significantly more negative (Figure 3a). This means that ERF$_{aci}$ due to Δf$_c$ dominates in clouds that are close to undergoing the breakup process in the observed world. Prior to ΔLWP ~100 g m^{-2}, the first indirect effect dominates with a weaker change in ERF$_{aci}$. This occurs when N$_d$ has experienced little scavenging (Figure 3d) and f$_c$ is still high (Figure 3c).
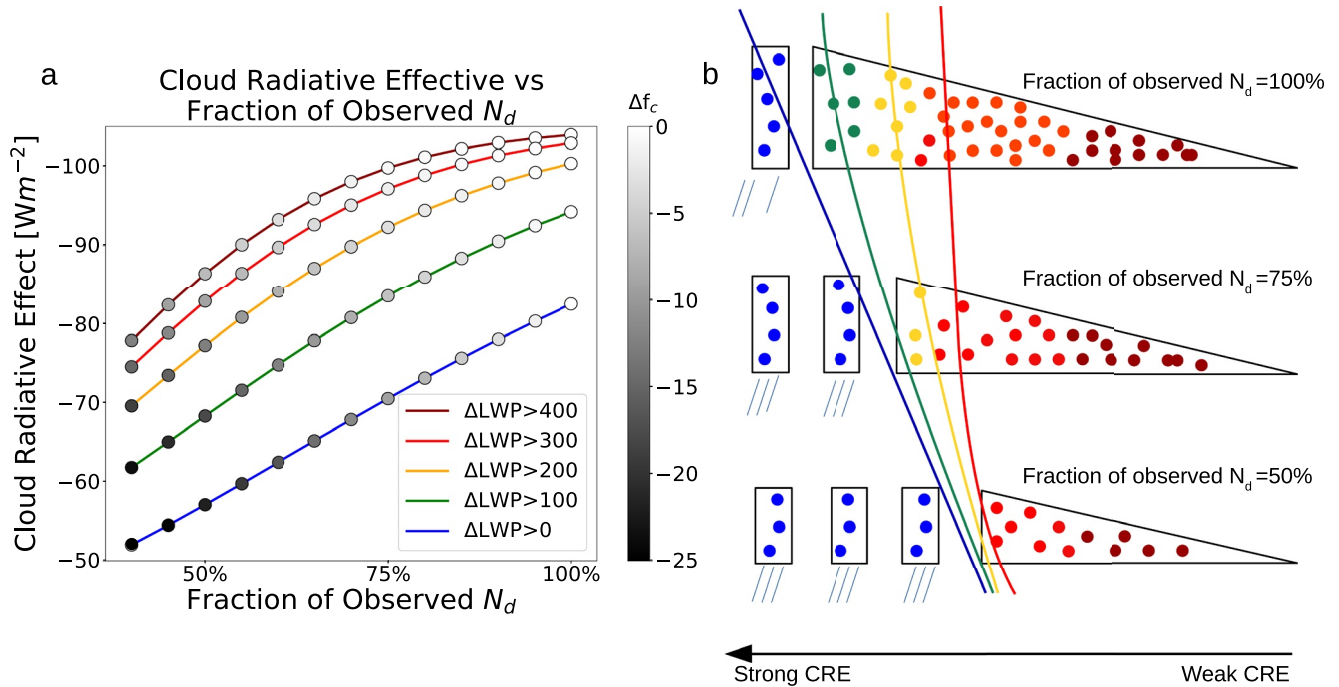
Figure 4. Transition from power-law to linear dependence of the cloud radiative effect (CRE) on N_d. (a) The CRE (curves, color coded according to the legend box) and Δf_c (points, according to the gray-scale color bar) with respect to a world consisting of different fractions of observed N_d. Each curve shows the mean CRE for data above a certain threshold of Δliquid water path (LWP). ΔLWP > 0 g m^{-2} includes observed solid clouds, with increasing thresholds representing clouds that are progressively further away in time and space from breakup. Note the shift from power-law (attributed to the weakening of the first indirect effect at higher N_d) to linear dependence of the CRE on fraction of observed N_d as soon as changes in f_c begin (gray-scale points). (b) Illustration of a stratocumulus cloud decks deck breaking up for different fractions of a given N_d (top to bottom). The CRE dependence on fraction of N_d is illustrated for several ΔLWP scenarios ranging from 300 g m^{-2} (red line) to 0 g m^{-2} (blue line), in accordance with the lines in (a) The ΔLWP of the illustrated lines represents the "observed" ΔLWP, that is, the cloud illustrated in the top panel. Note the retreat of the solid cloud deck under lower N_d due to a hastened breakup, which causes a linear dependence of the CRE on N_d (blue line), associated with the inherent near-linear dependence of CRE on f_c (Bender et al., 2011). Cloud droplets are colored by ΔLWP according to the color coded legend box in (a).

The strong decrease in the strength of ERF$_{aci}$ for ΔLWP < 0 g m^{-2} occurs because f_c is now sufficiently small such that there is little further leverage from a reduction in f_c, and there is a much smaller areal coverage for Twomey-brightening to act (Possner et al., 2018). A stronger decrease in f_c and CRE at lower N_d was also observed by (Rosenfeld et al., 2019).

3.2. Cloud Cover Response to N_d Mediates the Cloud Radiative Effect

Figure 4a shows the CRE (defined as the difference in all-sky shortwave radiation with respect to cloud-free conditions) as a function of fractions of observed N_d for clouds that correspond to certain ΔLWP thresholds (every ΔLWP threshold includes all clouds having ΔLWP above the threshold). Higher positive ΔLWP is associated with overcast clouds having high N_d. The N_d fractions range from 50 to 100% and are applied uniformly over the globe, allowing us to express the fundamental response of the CRE to changes in N_d. A power-law response of CRE to N_d fraction can be seen for ΔLWP > 400 gm^{-2}, which gradually becomes linear with decreasing threshold of ΔLWP. The transition from a power-law to a linear dependence of the CRE on N_d occurs when f_c (colored points in Figure 4a represent Δf_c) begins to respond to the lower N_d. The linearity results from the nearly linear relationship between f_c and $\bar{\alpha}$ shown in Figure 2a (Bender et al., 2011), which dominates the overall CRE of a given cloud scene. The CRE power-law dependence on N_d prior to the f_c change is attributed to the first indirect effect (Twomey, 1977), which depends on $N_d^{1/3}$ and therefore explains the weaker dependence on N_d when N_d is higher (Carslaw et al., 2013; Stevens, 2015; Twomey, 1991), as manifested by the higher thresholds of ΔLWP.

Figure 4b illustrates the power-law to linear transition of the CRE dependence on N_d by showing a Sc deck that breaks up sooner when the N_d is lower. The Sc deck is intended to resemble a climatological Sc deck in one of the major Sc regions, or under stable conditions elsewhere where meteorological conditions that favor Sc persist for several days (Goren & Rosenfeld, 2012, 2015). For high ΔLWP thresholds, clouds are overcast and the CRE

changes approximately according to the power-law dependence of the first indirect effect (red curve). When considering all of the observed solid clouds, that is, $\Delta LWP > 0$ g m^{-2}, Δf_c eventually dominates the response of the CRE to N_d, and a linear dependence emerges due to the consistent decrease in f_c (blue curve).

3.3. Realistic Global Effective Radiative Forcing Due To Delayed Sc Breakup

Here we estimate the global annual ERF$_{aci}$ due to delayed transitions by reducing the observed N_d to it's equivalent approximate in a pre-industrial world (see Section 3 in the Supporting Information S1 (S. Ghan et al., 2016; Gryspeerdt et al., 2016; Jia et al., 2021; McCoy et al., 2017; Yu & Luo, 2009; Quaas et al., 2008);). We find the global annual ERF$_{aci}$ due to delayed transitions to be −0.39 Wm^{-2} (0.34–0.42 Wm^{-2}) for all Sc clouds included in this study. We also calculated separately the ERF$_{aci}$ for Sc in the classic geographical Sc regions, as defined by the areas within the rectangles in Figure S2 in Supporting Information S1 (Muhlbauer et al., 2014). The latter is found to be −0.12 Wm^{-2} (0.11–0.13 Wm^{-2}). In these classic Sc regions persistent synoptic flow allows us to more confidently assume that the spatial climatology of the cloud properties is comparable to the Sc cloud properties along Lagrangian trajectories (see Section 2.3). For a discussion regarding the spatial pattern of the forcing, please refer to Section 6 in the Supporting Information S1. Note that the ERF$_{aci}$ is calculated for the data set from which the kernels are derived, and the uncertainty ranges account for the uncertainty in the kernels (Section 5.1 in the Supporting Information S1).

It should be emphasized that solid Sc can break up into open cells (Rosenfeld et al., 2006), become decoupled, and undergo the stratus-to-cumulus transition (Bretherton & Wyant, 1997; Wyant et al., 1997) or dissipate due to changing meteorology. Our assumption, that precipitation initiates the breakup (Goren et al., 2019; Rosenfeld et al., 2006; Wang & Feingold, 2009), means that allowing closed Sc cells that in reality undergo the stratus-to-cumulus transition to precipitate, would break them up into open cells before they reach the stratus-to-cumulus transition. We do note that precipitation may also accelerate the stratocumulus-to-cumulus transition directly (Yamaguchi et al., 2017), again suggesting an important, but unquantified role of the aerosol.

4. Conclusions

We find a linear response of Sc ERF$_{aci}$ to aerosol loading (represented here by N_d), with the ERF$_{aci}$ consisting of the f_c adjustment and the first indirect effect. The linearity emerges from (a) the consistent decrease in f_c accompanying decreasing N_d, and (b) the albedo being a near-linear function of f_c (Bender et al., 2011) (Figure 2a). Following this, closed-cells under high aerosol loading are advected further into the remote oceans as solid decks, instead of broken clouds. This results in increasing f_c that increases ERF$_{aci}$ linearly. For the current decreasing trend in anthropogenic aerosol emissions, this implies an acceleration of the warming due to greenhouse emissions, as the global Sc f_c is reduced along with the retreat of the Sc decks to their pre-industrial positions (assuming only changes in aerosol levels). Trend analyses of Sc cloud properties, to the extent records of satellite data allow, would provide observational evidence for our findings. It should be noted that other studies (Rotstayn et al., 2015; S. J. Ghan et al., 2013) have also shown a near-linear dependence of the forcing on emissions, however for the first indirect effect. The linearity in the latter studies was attributed to the spatio-temporal pattern of the aerosol emissions and transport (Kretzschmar et al., 2017).

We estimate the global ERF$_{aci}$ due to delayed Sc breakup to be −0.39 W m^{-2} with respect to PI aerosol levels. The ERF$_{aci}$ for the major Sc regions, where our assumptions of time and space equivalence can be more confidently defended (Sandu et al., 2010), is −0.12 W m^{-2}. An order of magnitude lower radiative effect was reported by Watson-Parris et al. (2021) for pocket of open cells (POCs), assuming the POCs would not be formed. The lower radiative effect was attributed to the lower frequency of occurrence of the POCs. The stronger forcing we find here provides a comprehensive assessment of the forcing due to closed cell breakup.

The f_c susceptibility to N_d is currently under-represented in the literature, and more importantly the strong reduction of f_c that occurs when $N_d < 50$ cm^{-3} is often neglected (Goren & Rosenfeld, 2014; Rosenfeld et al., 2019). Global climate models (GCMs) often assign a minimum N_d threshold to their simulations, as otherwise a strong cooling causes the simulations to diverge from observations (Hoose et al., 2009). The minimum N_d threshold corresponds to the N_d range over which Sc breakup occurs, which could be related to the GCMs underestimation of the negative ERF$_{aci}$ due to f_c change (Gryspeerdt et al., 2020; Mülmenstädt et al., 2021). Nevertheless, GCMs are the only tool to predict how Sc coverage will change in a future climate without simplified assumptions, as

done here. Our results therefore emphasize the need for improved GCM realism of warm, low level clouds and their interactions with aerosol, in order to provide a better estimate of future climate. Our metric can be used to evaluate model improvement using a process-oriented, observationally constrained metric.

Data Availability Statement

The MODIS aqua cloud products are available from the Atmosphere Archive and Distribution System (LAADS) Distributed Active Archive Center (DAAC): https://ladsweb.modaps.eosdis.nasa.gov/archive/allData/61/MOD06_L2/. The CERES SSF data are publicly available from NASA's Langley Research Center: https://ceres-tool.larc.nasa.gov/ord-tool/jsp/SSF1degEd41Selection.jsp. The fifth-generation European Center (ERA5) for Medium-range Weather Forecasts archive (ECMWF) data are available at: https://doi.org/10.24381/cds.bd0915c6. Simulation results and the anthropogenic droplet concentration fraction are available at: https://doi.org/10.5281/zenodo.7072605.

References

Albrecht, B. A. (1989). Aerosols, cloud microphysics, and fractional cloudiness. *Science*, *245*(4923), 1227–1230. https://doi.org/10.1126/science.245.4923.1227

Baker, M. B., & Charlson, R. J. (1990). Bistability of CCN concentrations and thermodynamics in the cloud-topped boundary layer. *Nature*, *345*(6271), 142–145. https://doi.org/10.1038/345142a0

Bender, F. A.-M., Charlson, R. J., Ekman, A. M., & Leahy, L. V. (2011). Quantification of monthly mean regional-scale albedo of marine stratiform clouds in satellite observations and GCMs. *Journal of Applied Meteorology and Climatology*, *50*(10), 2139–2148. https://doi.org/10.1175/jamc-d-11-049.1

Bender, F. A.-M., Engström, A., & Karlsson, J. (2016). Factors controlling cloud albedo in marine subtropical stratocumulus regions in climate models and satellite observations. *Journal of Climate*, *29*(10), 3559–3587. https://doi.org/10.1175/jcli-d-15-0095.1

Bennartz, R., & Rausch, J. (2017). Global and regional estimates of warm cloud droplet number concentration based on 13 years of AQUA-MODIS observations. *Atmospheric Chemistry and Physics*, *17*(16), 9815–9836. https://doi.org/10.5194/acp-17-9815-2017

Boucher, O., Randall, D., Artaxo, P., Bretherton, C., Feingold, G., Forster, P., et al. (2013). *Clouds and aerosols*. Cambridge University Press. https://doi.org/10.1017/CBO9781107415324.016

Brenguier, J.-L., Pawlowska, H., Schüller, L., Preusker, R., Fischer, J., & Fouquart, Y. (2000). Radiative properties of boundary layer clouds: Droplet effective radius versus number concentration. *Journal of the Atmospheric Sciences*, *57*(6), 803–821. https://doi.org/10.1175/1520-0469(2000)057<0803:rpoblc>2.0.co;2

Bretherton, C. S., Wood, R., George, R. C., Leon, D., Allen, G., & Zheng, X. (2010). Southeast Pacific stratocumulus clouds, precipitation and boundary layer structure sampled along 20 S during VOCALS-REx. *Atmospheric Chemistry and Physics Discussions*, *10*(6), 15921–15962. https://doi.org/10.5194/acp-10-10639-2010

Bretherton, C. S., & Wyant, M. C. (1997). Moisture transport, lower-tropospheric stability, and decoupling of cloud-topped boundary layers. *Journal of the Atmospheric Sciences*, *54*(1), 148–167. https://doi.org/10.1175/1520-0469(1997)054<0148:mtltsa>2.0.co;2

Carslaw, K. S., Lee, L. A., Reddington, C. L., Pringle, K. J., Rap, A., Forster, P. M., et al. (2013). Large contribution of natural aerosols to uncertainty in indirect forcing. *Nature*, *503*(7474), 67–71. https://doi.org/10.1038/nature12674

Chen, R., Wood, R., Li, Z., Ferraro, R., & Chang, F.-L. (2008). Studying the vertical variation of cloud droplet effective radius using ship and space-borne remote sensing data. *Journal of Geophysical Research*, *113*(D8), D00A02. https://doi.org/10.1029/2007jd009596

Christensen, M. W., Jones, W. K., & Stier, P. (2020). Aerosols enhance cloud lifetime and brightness along the stratus-to-cumulus transition. *Proceedings of the National Academy of Sciences*, *117*(30), 17591–17598. https://doi.org/10.1073/pnas.1921231117

Diamond, M. S., Saide, P. E., Zuidema, P., Ackerman, A. S., Doherty, S. J., Fridlind, A. M., et al. (2022). Cloud adjustments from large-scale smoke-circulation interactions strongly modulate the southeast Atlantic stratocumulus-to-cumulus transition. *Atmospheric Chemistry and Physics Discussions*, *22*(18), 1–57. https://doi.org/10.5194/acp-22-12113-2022

Engström, A., Bender, F.-M., Charlson, R., & Wood, R. (2015). The nonlinear relationship between albedo and cloud fraction on near-global, monthly mean scale in observations and in the CMIP5 model ensemble. *Geophysical Research Letters*, *42*(21), 9571–9578. https://doi.org/10.1002/2015gl066275

Feingold, G., Balsells, J., Glassmeier, F., Yamaguchi, T., Kazil, J., & McComiskey, A. (2017). Analysis of albedo versus cloud fraction relationships in liquid water clouds using heuristic models and large eddy simulation. *Journal of Geophysical Research: Atmospheres*, *122*(13), 7086–7102. https://doi.org/10.1002/2017jd026467

Feingold, G., Koren, I., Wang, H., Xue, H., & Brewer, W. A. (2010). Precipitation-generated oscillations in open cellular cloud fields. *Nature*, *466*(7308), 849–52. https://doi.org/10.1038/nature09314

Forster, P., Storelvmo, T., Armour, K., Collins, W., Dufresne, J.-L., Frame, D., et al. (2021). The earth's energy budget, climate feedbacks, and climate sensitivity.

Freud, E., & Rosenfeld, D. (2012). Linear relation between convective cloud drop number concentration and depth for rain initiation. *Journal of Geophysical Research*, *117*(2), 1–13. https://doi.org/10.1029/2011JD016457

Gerber, H. (1996). Microphysics of marine stratocumulus clouds with two drizzle modes. *Journal of the Atmospheric Sciences*, *53*(12), 1649–1662. https://doi.org/10.1175/1520-0469(1996)053<1649:momscw>2.0.co;2

Ghan, S., Wang, M., Zhang, S., Ferrachat, S., Gettelman, A., Griesfeller, J., et al. (2016). Challenges in constraining anthropogenic aerosol effects on cloud radiative forcing using present-day spatiotemporal variability. *Proceedings of the National Academy of Sciences of United States of America*, *113*(21), 5804–5811. https://doi.org/10.1073/pnas.1514036113

Ghan, S. J., Smith, S. J., Wang, M., Zhang, K., Pringle, K., Carslaw, K., et al. (2013). A simple model of global aerosol indirect effects. *Journal of Geophysical Research: Atmospheres*, *118*(12), 6688–6707. https://doi.org/10.1002/jgrd.50567

Goren, T., Kazil, J., Hoffmann, F., Yamaguchi, T., & Feingold, G. (2019). Anthropogenic air pollution delays marine stratocumulus breakup to open cells. *Geophysical Research Letters*, *46*(23), 14135–14144. https://doi.org/10.1029/2019gl085412

Goren, T., & Rosenfeld, D. (2012). Satellite observations of ship emission induced transitions from broken to closed cell marine stratocumulus over large areas. *Journal of Geophysical Research*, *117*(D17). https://doi.org/10.1029/2012jd017981

Goren, T., & Rosenfeld, D. (2014). Decomposing aerosol cloud radiative effects into cloud cover, liquid water path and Twomey components in marine stratocumulus. *Atmospheric Research*, *138*, 378–393. https://doi.org/10.1016/j.atmosres.2013.12.008

Goren, T., & Rosenfeld, D. (2015). Extensive closed cell marine stratocumulus downwind of Europe-A large aerosol cloud mediated radiative effect or forcing? *Journal of Geophysical Research: Atmospheres*, *120*(12), 6098–6116. https://doi.org/10.1002/2015JD023176

Grosvenor, D., & Wood, R. (2014). The effect of solar zenith angle on MODIS cloud optical and microphysical retrievals within marine liquid water clouds. *Atmospheric Chemistry and Physics*, *14*(14), 7291–7321. https://doi.org/10.5194/acp-14-7291-2014

Grosvenor, D. P., Sourdeval, O., Zuidema, P., Ackerman, A., Alexandrov, M. D., Bennartz, R., et al. (2018). Remote sensing of droplet number concentration in warm clouds: A review of the current state of knowledge and perspectives. *Reviews of Geophysics*, *56*(2), 409–453. https://doi.org/10.1029/2017RG000593

Gryspeerdt, E., Mülmenstädt, J., Gettelman, A., Malavelle, F. F., Morrison, H., Neubauer, D., et al. (2020). Surprising similarities in model and observational aerosol radiative forcing estimates. *Atmospheric Chemistry and Physics*, *20*(1), 613–623. https://doi.org/10.5194/acp-20-613-2020

Gryspeerdt, E., Quaas, J., & Bellouin, N. (2016). Constraining the aerosol influence on cloud fraction. *Journal of Geophysical Research: Atmospheres*, *121*(7), 3566–3583. https://doi.org/10.1002/2015jd023744

Hoose, C., Kristjánsson, J., Iversen, T., Kirkevåg, A., Seland, Ø., & Gettelman, A. (2009). Constraining cloud droplet number concentration in GCMs suppresses the aerosol indirect effect. *Geophysical Research Letters*, *36*(12), L12807. https://doi.org/10.1029/2009gl038568

Jia, H., Ma, X., Yu, F., & Quaas, J. (2021). Significant underestimation of radiative forcing by aerosol–cloud interactions derived from satellite-based methods. *Nature Communications*, *12*(1), 1–11. https://doi.org/10.1038/s41467-021-23888-1

Khairoutdinov, M. F., & Randall, D. A. (2003). Cloud resolving modeling of the ARM summer 1997 IOP: Model formulation, results, uncertainties, and sensitivities. *Journal of the Atmospheric Sciences*, *60*(4), 607–625. https://doi.org/10.1175/1520-0469(2003)060<0607:crmota>2.0.co;2

Koren, I., & Feingold, G. (2011). Aerosol–cloud–precipitation system as a predator-prey problem. *Proceedings of the National Academy of Sciences*, *108*(30), 12227–12232. https://doi.org/10.1073/pnas.1101777108

Kretzschmar, J., Salzmann, M., Mülmenstädt, J., Boucher, O., & Quaas, J. (2017). Comment on "rethinking the lower bound on aerosol radiative forcing". *Journal of Climate*, *30*(16), 6579–6584. https://doi.org/10.1175/jcli-d-16-0668.1

McCoy, D., Bender, F.-M., Mohrmann, J., Hartmann, D., Wood, R., & Grosvenor, D. (2017). The global aerosol-cloud first indirect effect estimated using MODIS, MERRA, and AeroCom. *Journal of Geophysical Research: Atmospheres*, *122*(3), 1779–1796. https://doi.org/10.1002/2016jd026141

Muhlbauer, A., McCoy, I. L., & Wood, R. (2014). Climatology of stratocumulus cloud morphologies: Microphysical properties and radiative effects. *Atmospheric Chemistry and Physics*, *14*(13), 6695–6716. https://doi.org/10.5194/acp-14-6695-2014

Mülmenstädt, J., Salzmann, M., Kay, J. E., Zelinka, M. D., Ma, P.-L., Nam, C., et al. (2021). An underestimated negative cloud feedback from cloud lifetime changes. *Nature Climate Change*, *11*(6), 508–513. https://doi.org/10.1038/s41558-021-01038-1

Platnick, S., King, M., Ackerman, S., Menzel, W., Baum, B., Riedi, J., & Frey, R. (2003). The MODIS cloud products: Algorithms and examples from terra. *IEEE Transactions on Geoscience and Remote Sensing*, *41*(2), 459–473. https://doi.org/10.1109/TGRS.2002.808301

Possner, A., Wang, H., Wood, R., Caldeira, K., & Ackerman, T. P. (2018). The efficacy of aerosol–cloud radiative perturbations from near-surface emissions in deep open-cell stratocumuli. *Atmospheric Chemistry and Physics*, *18*(23), 17475–17488. https://doi.org/10.5194/acp-18-17475-2018

Quaas, J., Boucher, O., Bellouin, N., & Kinne, S. (2008). Satellite-based estimate of the direct and indirect aerosol climate forcing. *Journal of Geophysical Research*, *113*(D5). https://doi.org/10.1029/2007jd008962

Quaas, J., Boucher, O., & Lohmann, U. (2006). Constraining the total aerosol indirect effect in the LMDZ and ECHAM4 GCMs using MODIS satellite data. *Atmospheric Chemistry and Physics*, *6*(4), 947–955. https://doi.org/10.5194/acp-6-947-2006

Rosenfeld, D., Kaufman, Y. J., & Koren, I. (2006). Switching cloud cover and dynamical regimes from open to closed Benard cells in response to the suppression of precipitation by aerosols. *Atmospheric Chemistry and Physics*, *6*(9), 2503–2511. https://doi.org/10.5194/acp-6-2503-2006

Rosenfeld, D., Wang, H., & Rasch, P. J. (2012). The roles of cloud drop effective radius and LWP in determining rain properties in marine stratocumulus. *Geophysical Research Letters*, *39*(13). https://doi.org/10.1029/2012GL052028

Rosenfeld, D., Zhu, Y., Wang, M., Zheng, Y., Goren, T., & Yu, S. (2019). Aerosol-driven droplet concentrations dominate coverage and water of oceanic low-level clouds. *Science*, *363*(6427), eaav0566. https://doi.org/10.1126/science.aav0566

Rotstayn, L. D., Collier, M. A., Shindell, D. T., & Boucher, O. (2015). Why does aerosol forcing control historical global-mean surface temperature change in CMIP5 models? *Journal of Climate*, *28*(17), 6608–6625. https://doi.org/10.1175/jcli-d-14-00712.1

Sandu, I., Stevens, B., & Pincus, R. (2010). On the transitions in marine boundary layer cloudiness. *Atmospheric Chemistry and Physics*, *10*(5), 2377–2391. https://doi.org/10.5194/acp-10-2377-2010

Schneider, S. H., & Dickinson, R. E. (1976). Parameterization of fractional cloud amounts in climatic models: The importance of modeling multiple reflections. *Journal of Applied Meteorology and Climatology*, *15*(10), 1050–1056. https://doi.org/10.1175/1520-0450(1976)015<1050:pofcai>2.0.co;2

Sharon, T. M., Albrecht, B. A., Jonsson, H. H., Minnis, P., Khaiyer, M. M., van Reken, T. M., et al. (2006). Aerosol and cloud microphysical characteristics of rifts and gradients in maritime stratocumulus clouds. *Journal of the Atmospheric Sciences*, *63*(3), 983–997. https://doi.org/10.1175/JAS3667.1

Slingo, A. (1990). Sensitivity of the Earth's radiation budget to changes in low clouds. *Nature*, *343*(6253), 49–51. https://doi.org/10.1038/343049a0

Sourdeval, O., Labonnote, L. C., Baran, A. J., Mülmenstädt, J., & Brogniez, G. (2016). A methodology for simultaneous retrieval of ice and liquid water cloud properties. Part 2: Near-global retrievals and evaluation against A-Train products. *Quarterly Journal of the Royal Meteorological Society*, *142*(701), 3063–3081. https://doi.org/10.1002/qj.2889

Stevens, B. (2015). Rethinking the lower bound on aerosol radiative forcing. *Journal of Climate*, *28*(12), 4794–4819. https://doi.org/10.1175/JCLI-D-14-00656.1

Twomey, S. (1977). The influence of pollution on the shortwave albedo of clouds. *Journal of the Atmospheric Sciences*, *34*(7), 1149–1152. https://doi.org/10.1175/1520-0469(1977)034<1149:tiopot>2.0.co;2

Twomey, S. (1991). Aerosols, clouds and radiation. *Atmospheric Environment, Part A: General Topics*, *25*(11), 2435–2442. https://doi.org/10.1016/0960-1686(91)90159-5

VanZanten, M. C., Stevens, B., Vali, G., & Lenschow, D. H. (2005). Observations of drizzle in nocturnal marine stratocumulus. *Journal of the Atmospheric Sciences*, *62*(1), 88–106. https://doi.org/10.1175/jas-3355.1

Wang, H., & Feingold, G. (2009). Modeling mesoscale cellular structures and drizzle in marine stratocumulus. Part I: Impact of drizzle on the formation and evolution of open cells. *Journal of the Atmospheric Sciences*, *66*(11), 3237–3256. https://doi.org/10.1175/2009JAS3022.1

Wang, H., Feingold, G., Wood, R., & Kazil, J. (2010). Modelling microphysical and meteorological controls on precipitation and cloud cellular structures in Southeast Pacific stratocumulus. *Atmospheric Chemistry and Physics*, *10*(13), 6347–6362. https://doi.org/10.5194/acp-10-6347-2010

Watson-Parris, D., Sutherland, S., Christensen, M., Eastman, R., & Stier, P. (2021). A large-scale analysis of pockets of open cells and their radiative impact. *Geophysical Research Letters*, *48*(6), e2020GL092213. https://doi.org/10.1029/2020gl092213

Wielicki, B. A., Barkstrom, B. R., Harrison, E. F., Lee, R. B., III, Smith, G. L., & Cooper, J. E. (1996). Clouds and the Earth's radiant energy system (CERES): An Earth observing system experiment. *Bulletin of the American Meteorological Society*, *77*(5), 853–868. https://doi.org/10.1175/1520-0477(1996)077<0853:catere>2.0.co;2

Wood, R. (2012). Stratocumulus clouds. *Monthly Weather Review*, *140*(8), 2373–2423. https://doi.org/10.1175/mwr-d-11-00121.1

Wood, R., Bretherton, C. S., Leon, D., Clarke, a. D., Zuidema, P., Allen, G., & Coe, H. (2011). An aircraft case study of the spatial transition from closed to open mesoscale cellular convection over the Southeast Pacific. *Atmospheric Chemistry and Physics*, *11*(5), 2341–2370. https://doi.org/10.5194/acp-11-2341-2011

Wyant, M. C., Bretherton, C. S., Rand, H. A., & Stevens, D. E. (1997). Numerical simulations and a conceptual model of the stratocumulus to trade cumulus transition. *Journal of the Atmospheric Sciences*, *54*(1), 168–192. https://doi.org/10.1175/1520-0469(1997)054<0168:nsaacm>2.0.co;2

Yamaguchi, T., Feingold, G., & Kazil, J. (2017). Stratocumulus to cumulus transition by drizzle. *Journal of Advances in Modeling Earth Systems*, *9*(6), 2333–2349. https://doi.org/10.1002/2017MS001104

Yu, F., & Luo, G. (2009). Simulation of particle size distribution with a global aerosol model: Contribution of nucleation to aerosol and CCN number concentrations. *Atmospheric Chemistry and Physics*, *9*(20), 7691–7710. https://doi.org/10.5194/acp-9-7691-2009